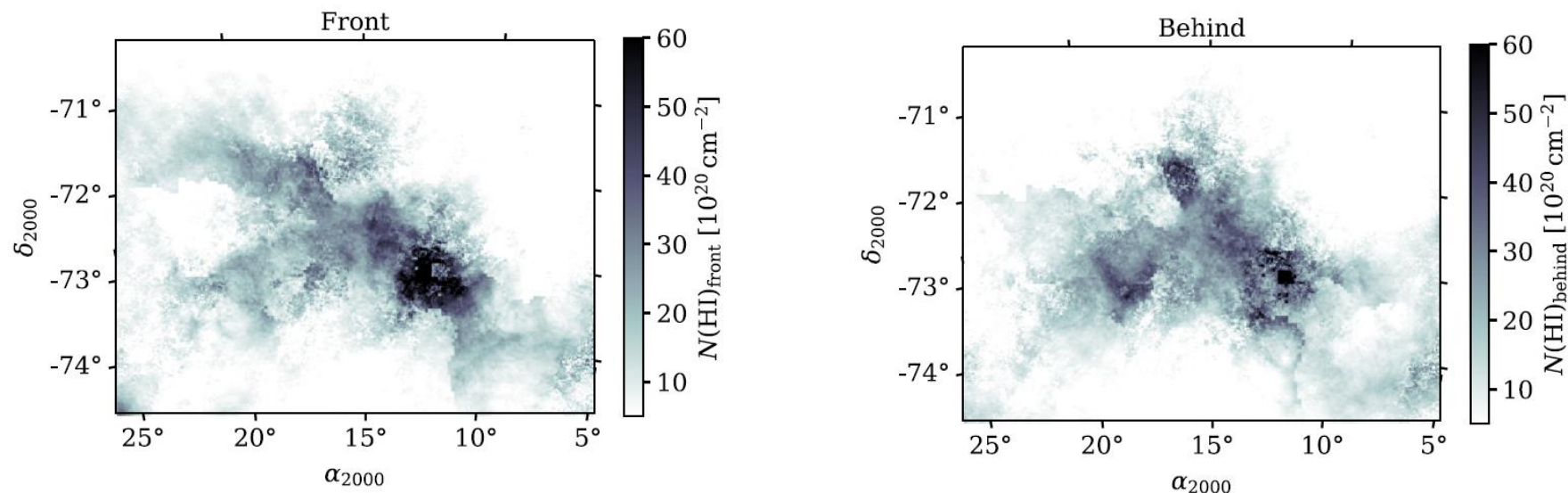




A Galactic Eclipse: The Small Magellanic Cloud Is Forming Stars in Two Superimposed Systems

Claire E. Murray^{1,2} , Sten Hasselquist¹ , Joshua E. G. Peek^{1,2} , Christina Willecke Lindberg^{1,2} , Andres Almeida³ , Yumi Choi⁴ , Jessica E. M. Craig⁵ , Helga Dénes⁶ , John M. Dickey⁷ , Enrico M. Di Teodoro⁸ , Christoph Federrath^{9,10} , Isabella. A. Gerrard⁹ , Steven J. Gibson¹¹ , Denis Leahy¹² , Min-Young Lee^{13,14} , Callum Lynn⁹ , Yik Ki Ma⁹ , Antoine Marchal⁹ , N. M. McClure-Griffiths⁹ , David Nidever¹⁵ , Hiep Nguyen⁹ , Nickolas M. Pingel¹⁶ , Elizabeth Tarantino¹ , Lucero Uscanga¹⁷ , and Jacco Th. van Loon⁵



Aims

This work wants to demonstrate the SMC is actually composed of **two superimposed star forming systems** with similar gas mass **separated by ~ 5 kpc**

Data

Galactic Australian Square Kilometer Array Pathfinder (GASKAP) + radial velocities from Gaia and APOGEE

Main topics

1. Structure and dynamics of the **Star Forming Disk** of the **Small Magellanic Cloud (SMC)**
2. Interstellar Medium (ISM) traced by the emission by **neutral atomic hydrogen (HI)**
3. **Young Massive Stars**
4. **Dust extinction**

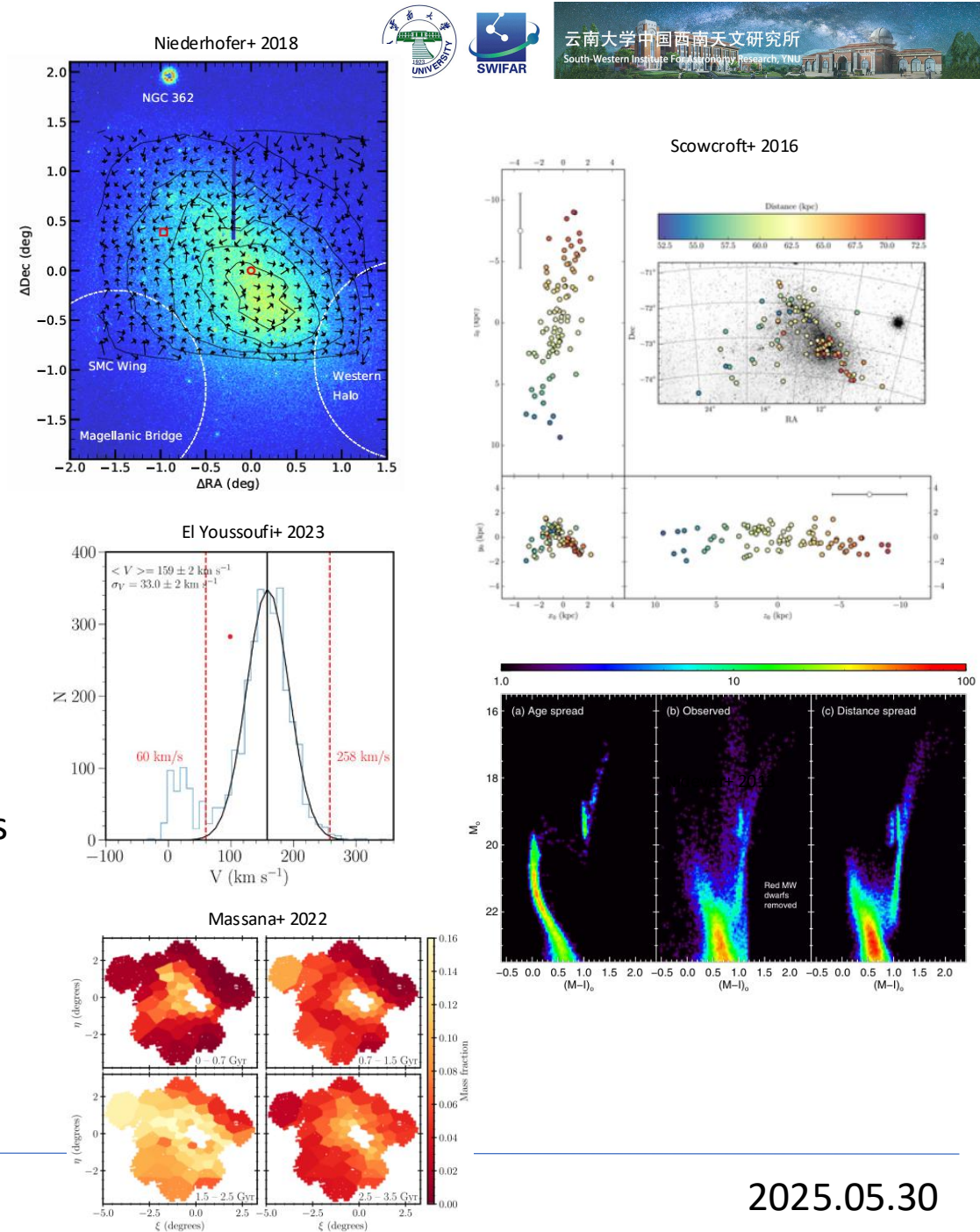
The SMC is among the largest satellite galaxies of the Milky Way (MW). It displays an apparent size of $\sim 5.3^\circ \times 3^\circ$, which at a distance of about 62 kpc corresponds to an (isophotal) extension of ~ 5.8 kpc ($\sim 1/40_{\text{th}}$ of the MW). It has a mass of $7 \times 10^9 M_\odot$, somewhat lower than the Large Magellanic Cloud (LMC; $\sim 10^{10} M_\odot$)

The SMC is a particularly interesting object because it shows very different conditions from those typically found in the MW. There are active star forming regions (in the South-Western bar) with abundant molecular gas, with metallicity as low as $0.2 Z_\odot$. Because of its relatively low distance – compared to that of other distance galaxies – stars can still be resolved thus allowing to study the conditions of the interstellar medium and star formation similar to those present at high redshifts ($z \sim 2 - 3$) in the early Universe!



Line of sight structure of the SMC

1. Old stellar population: spherically distributed within a radius of 7-12 kpc (e.g Niederhofer+ 2018) with no sign of rotation except for the central (± 1 kpc from the center)
2. Stars with measurable distance (Cepheid, RR Lyrae) are dispersed along the line of sight with a depth of 20-30 kpc (e.g. Scowcroft+ 2016)
3. Young Main Sequence and Red Giant Stars (RGB) display a radial velocity gradient indicative of rotation (e.g. El Youssefi+ 2023)
4. Distinct substructures along the line of sight traced by Red Clump stars, which show a sort of bimodality (e.g. Nidever+ 2013)
5. RGB complex distribution in radial velocity and metallicity suggests a non-uniform chemical enrichment either due to subsequent star formation bursts (e.g. Massana+ 2022) or chemically distinct substructures



Line of sight structure of the SMC

1. Highly disturbed ISM: HI emission in the SMC shows multiple peaks on radial velocity – originally interpreted as due to the presence of two subsystems separated in space (e.g. Hindman 1964)
2. Velocity of stars, HII regions, and planetary nebulae follow that of the HI emission, leading to the conclusion that the SMC was torn by interaction with the LMC (e.g. Murai & Fujimoto 1980)
3. The common interpretation is that low velocity gas lies in front because optical absorption is associated with the low-velocity HI peak. However recent studies show that filaments in low- and high-velocity components appear aligned with each other suggesting a physical relation among them (Ma+ 2023).
Alternatively, the filaments would form a series of overlapping supershells
4. Despite the aforementioned complexity, the velocity field of the SMC is consistent with that of a rotating disk

Hindman 1964

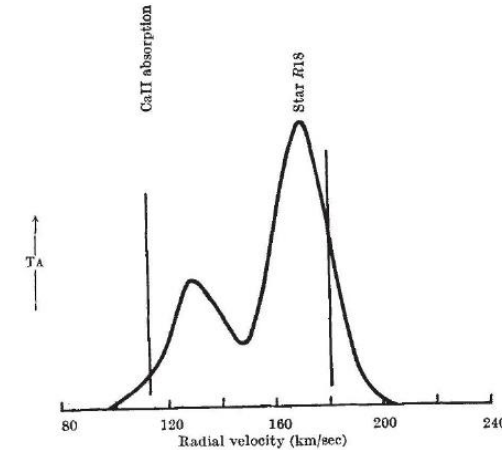


Fig. 2. Sample double-peaked profile at R.A. 0059-2, dec. $-72^{\circ} 29'$ (1975). The velocities of the star *R18* in the Radcliffe list and associated CaII absorption are marked

Ma+ 2023

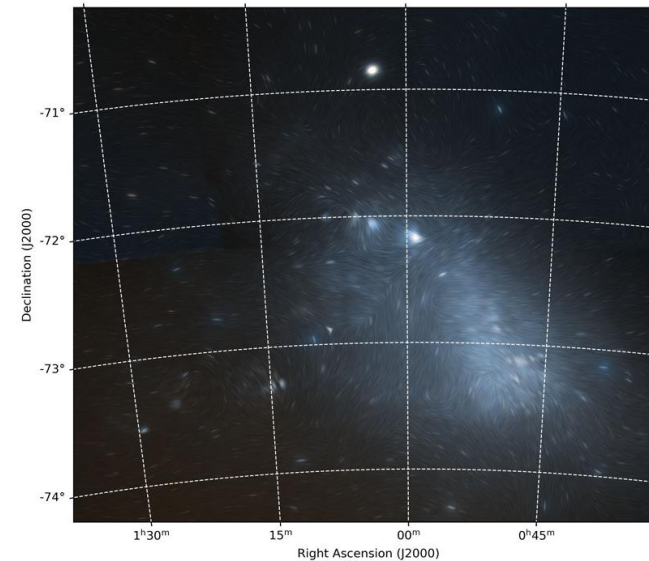


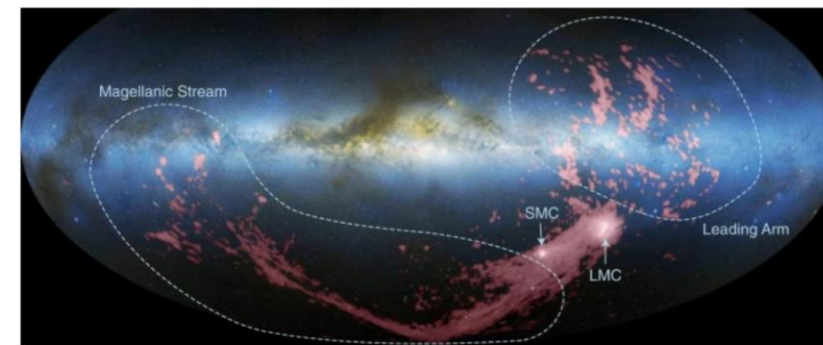
Figure 10. Result of ray tracing through the low-velocity portion (presumably the near-side of the SMC) of the GASKAP-HI data cube, with the effect of starlight attenuation due to dust extinction taken into account. The position angle is shown as the flow-line pattern generated by the LIC algorithm (Cabral & Lendon 1993). This can be compared with future starlight polarization observations to test whether H I filaments are aligned with the magnetic field throughout the entirety of the SMC. The colour optical map is from the Digitized Sky Surveys 2 (DSS2; Lasker et al. 1996).

Line of sight structure of the SMC

However, there are some discrepancies:

- HI velocity gradient perpendicular to that of young stars
- Distance gradient of Cepheids oriented 90 degrees from the minor axis of the gas disk
- 3D kinematics of young, massive stars (young enough to trace the kinematics of their birth clouds) are inconsistent with a rotating disk model

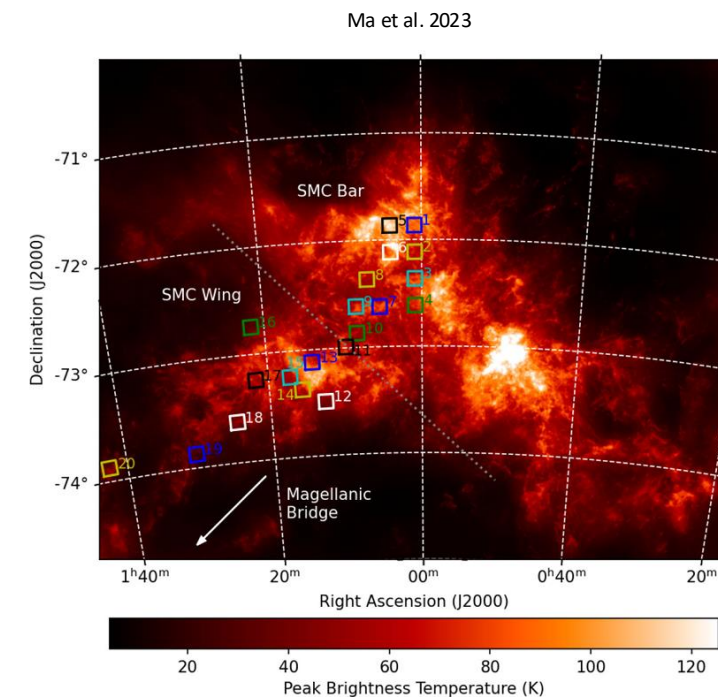
A general explanation to reconcile the observational discrepancies relies on the assumption that the LMC and SMC had a complex interaction history during the last Gyrs and that this have produced a wealth of debris in the outskirts of both the clouds. In particular, according to the latest models the LMC and SMC collided about 150 Myr ago producing debris fields like the Bridge, the Leading Arm and the Stream



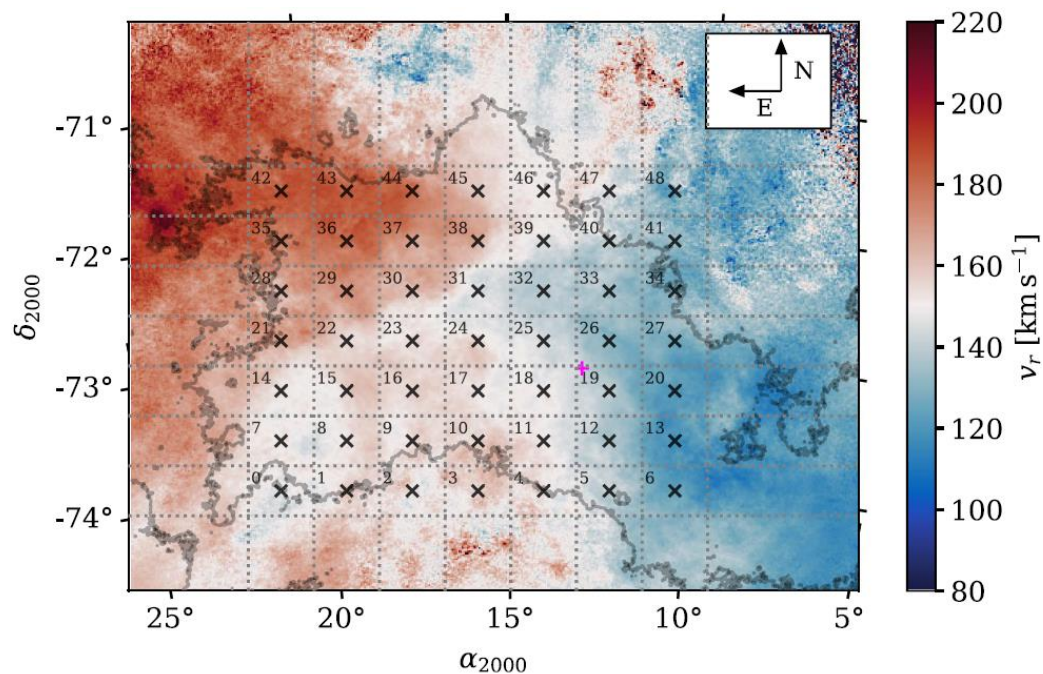
Credit: Image adapted from [D. L. Nidever et al. *Astrophys. J.* **723**, 1618–1631 \(2010\)](#), AAS/IOP.

Data

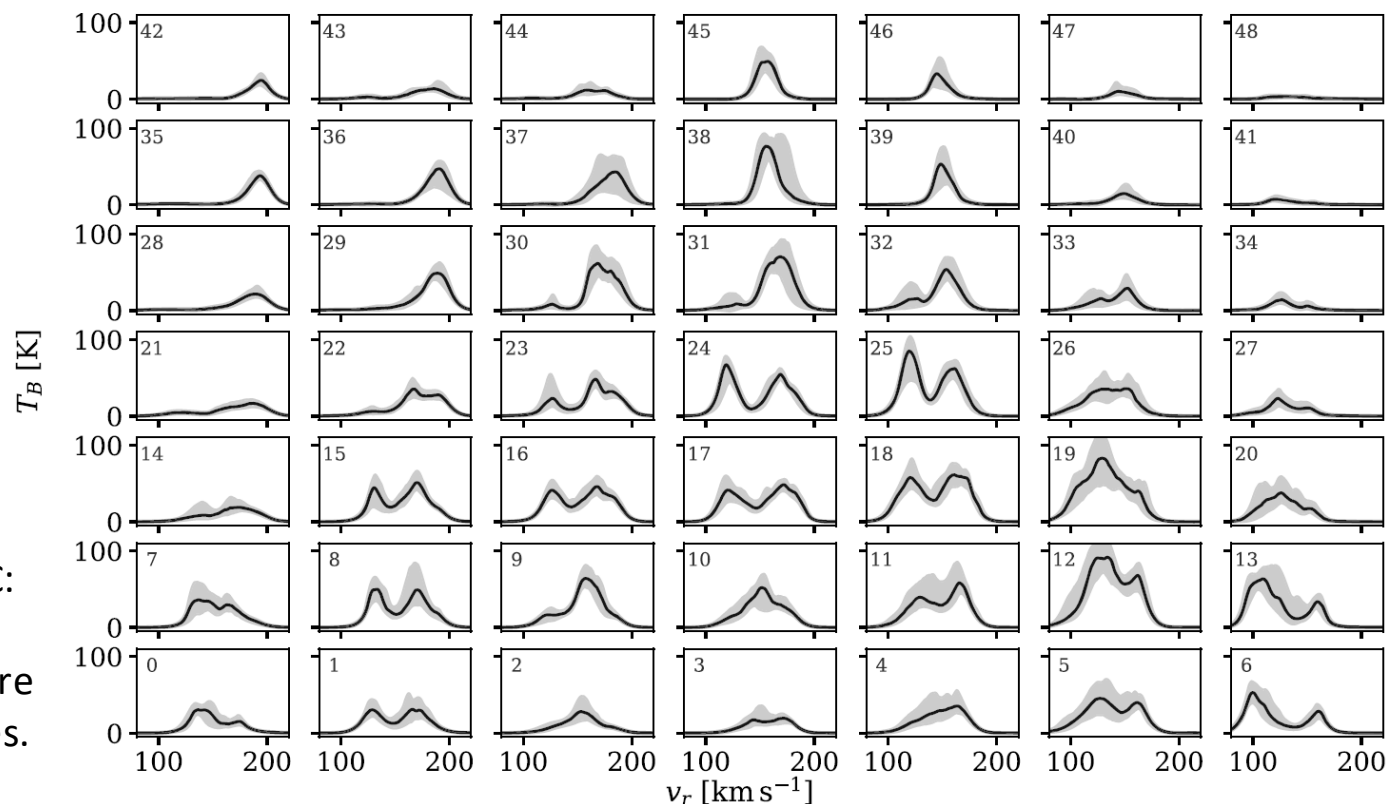
1. High-resolution observations of the SMC's neutral gas emission at 21 cm from the Galactic Australian Square Kilometer Array Pathfinder (GASKAP-H I) survey (Pingel et al. 2022), which trace the radial velocity of the bulk gas population in the system
2. Line-of-sight extinction and radial velocity measurements of bright, young (10–100 Myr) stars in the SMC from the Gaia mission DR3
3. APOGEE spectral fits, as well as large-area molecular gas observations of the system to assess its chemical state



Intensity-weighted mean radial velocity of the GASKAP-H I cube



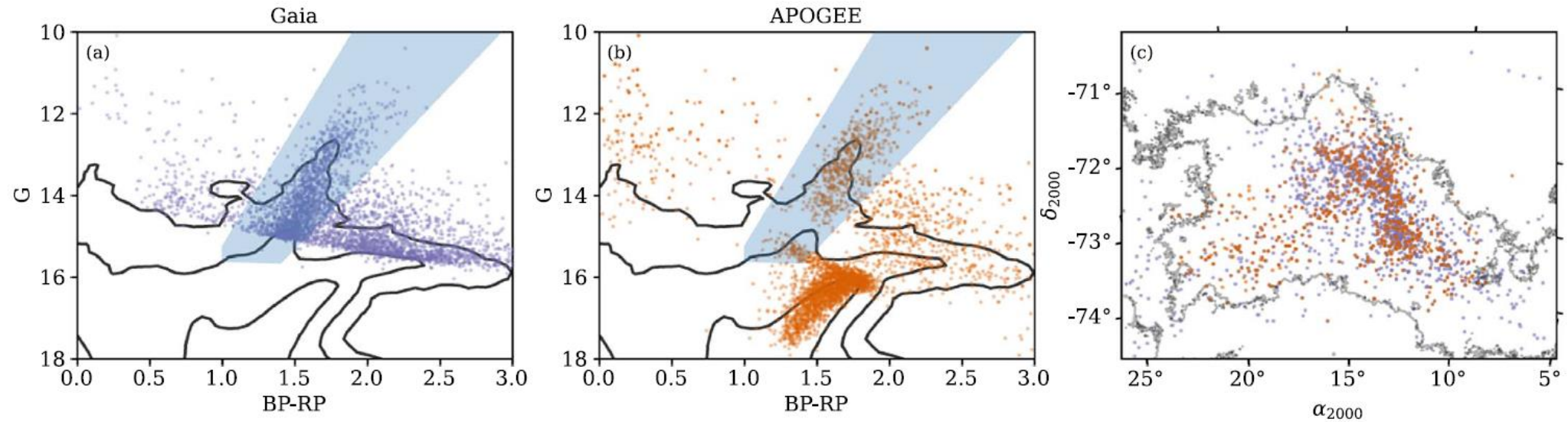
The map shows of the velocity structure of gas in the SMC: a clear gradient is visible, consistent with a rotating disk. However, a gradient is visible in the Brightness Temperature spectra T_b , which shows a complex multi-peaked structures. In particular, across the SMC main body, two different spectral components (130 and 170 km/s) are visible



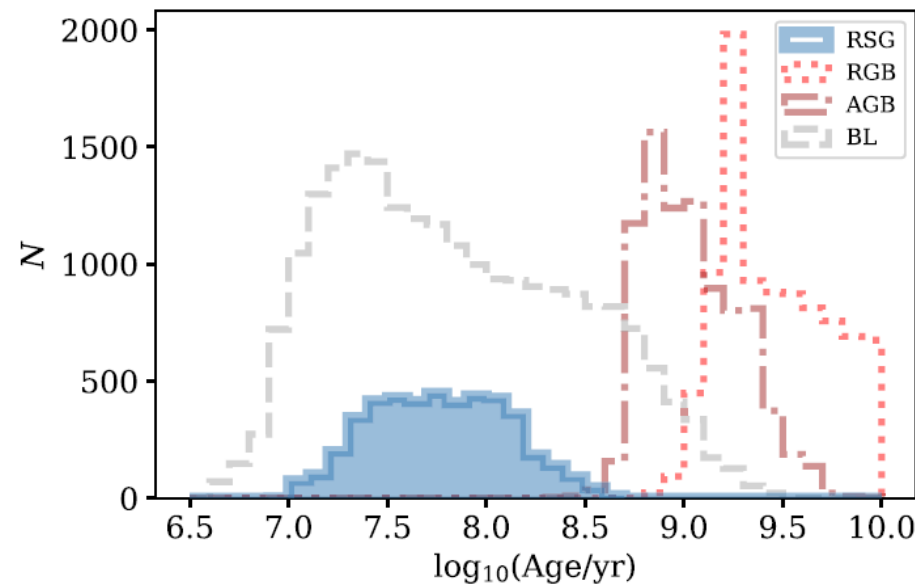
Selection requirements for the Gaia and APOGEE stellar samples

- The 21 cm emission provides a high-resolution probe of the position–velocity structure of the gas, but not the line-of-sight distance axis, therefore to sample this third spatial dimension, it is necessary to use measurements of extinction by dust toward individual stars, because extinction provides a cumulative measurement of the effect of dust along the line of sight
- By comparing extinction values toward stars at different radial velocities it is possible to determine the relative spatial order of these stars along the line of sight (i.e., “front” and “behind”)
- The primary goal is to connect the line-of-sight structure of the stars with the radial velocity structure of the gas, by assuming that gas, dust, and young stars coexist spatially and share bulk kinematics on the same spatial scales probed by each tracer.
- Although the assumption that dust and gas are well mixed is widely accepted, the assumption that the stars trace the same 3D motions as the gas relies on targeting only the youngest stellar populations, whose lives are short enough that their motions are coupled to the motions of their parent gas clouds.
- Since the precise definition of “young” to satisfy the above requirement is not well defined in the SMC low-metallicity and dynamically complex environment, the young star sample contains stars of a few tens of Myrs, an age that is somewhat smaller than the SMC dynamical timescale (crossing time) of ~ 100 Myr

Color-Magnitude diagrams and spatial distribution of the selected young stars



In the case of the Gaia sample, the stars with measured radial velocities are all bright. In both samples, the stars span a wide range of stellar types, including pulsating variables, red supergiants (RSGs), and asymptotic giant branch (AGB) stars. The APOGEE stars span a wider range in magnitude, as this survey included both shallow and deep observations. As a result, there is a gap between the faintest and brightest RSGs around $G \sim 15$. A further selection is therefore necessary to: 1) identify stars that are young enough to support the assumption that their motions trace the bulk motions of their parent gas clouds; 2) stars of a spectral type that is well understood enough for the line-of-sight extinction toward them to be accurately inferred with available data. The blue area satisfies these criteria. This region of the CMD is indeed dominated by RSGs.

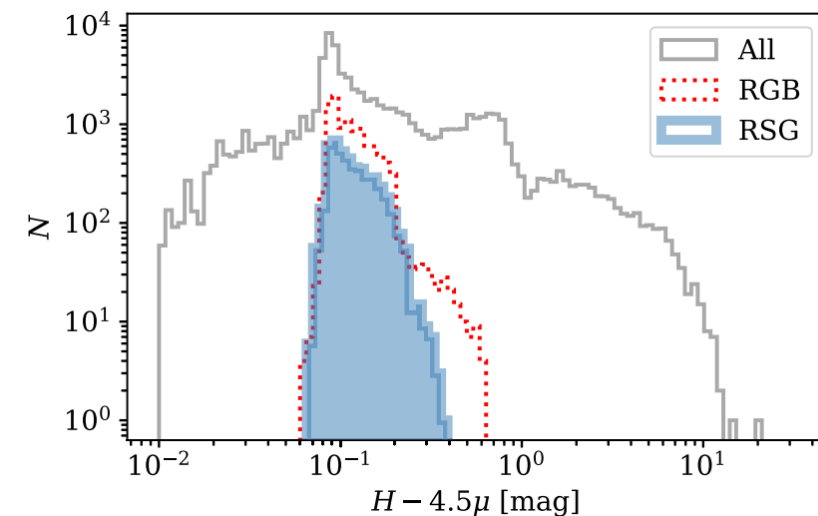


A set of synthetic stellar isochrone tables for a range of SMC metallicities ($[M/H] = -1.0$ to -0.65) from PARSEC (Bressan + 2012) has been generated and various age distributions have been extracted. The histograms of the ages of stars in the RSG selection (blue), as well as the ages of a range of stellar populations identified in the SMC by Gaia Collaboration et al. (2021), including RGB, AGB, and blue loop (BL) stars. The RSGs are of intermediate age ($\sim 10 - 100$ Myr) but are among the youngest stars available in the two surveys. In addition, RSGs in the LMC have been shown to closely mimic the kinematics of the H I (Olsen + 2015). Following the RSG selection, the Gaia and APOGEE catalogues have been cross-matched the catalogs resulting in a total of 1947 stars (782 APOGEE, 1165 Gaia). Because the APOGEE survey of the SMC was limited to individual pointings, these stars are not uniformly spread across the galaxy like the Gaia stars

Extinction estimates

- To estimate the extinction toward each source in the sample it was used the Rayleigh–Jeans color excess (RJCE) method (Majewski et al. 2011). RJCE was developed to quantify the amount of reddening toward individual stars based on a single observed color, $H - 4.5 \mu\text{m}$. These wavelengths sample the Rayleigh–Jeans tail of the stellar spectral energy distribution, where red clump and red giant stars have the same intrinsic color. As a result, **variations in their observed colors can be attributed to the effect of dust extinction**
- Since the RJCE method has not been explicitly validated on RSG, in order to test the validity of the method, the same set of synthetic isochrones were used to plot the histograms of the $H - 4.5\mu\text{m}$ colors for the RSG sample compared with the RGB sample (where the color–magnitude selection for SMC RGBs is defined in Gaia Collaboration et al. (2021))
- It can be seen that the RSG-selected stars span an even narrower $H - 4.5\mu\text{m}$ color range than the RGB stars thus validating the use of the RJCE method
- Extinction was computed by using the Spitzer catalogs from the SAGE-SMC survey data, which include $4.5 \mu\text{m}$ photometry. Extinction in K_s band was obtained with the relation

$$A_K = 0.918 (H - [4.5\mu] - 0.08)$$



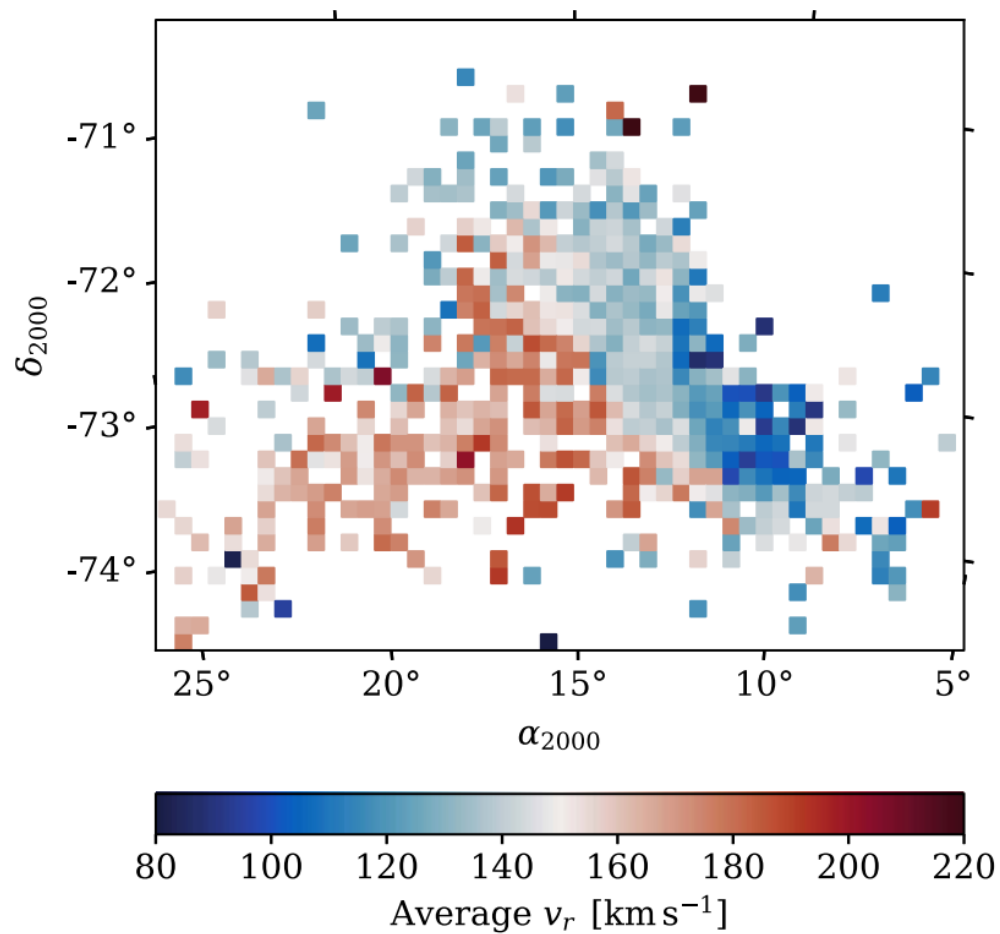
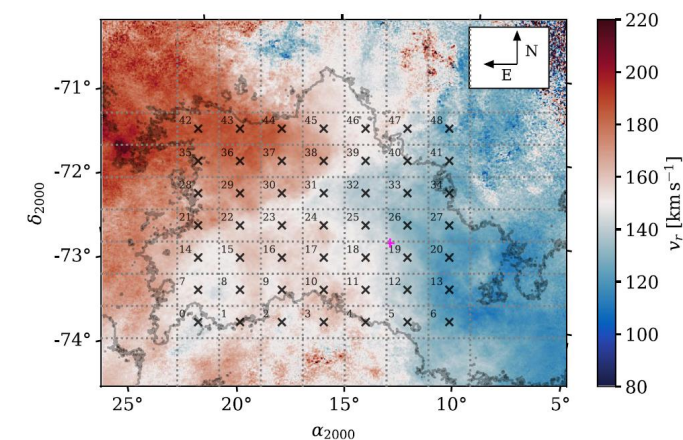


Figure 5. Average radial velocity of the selected stellar catalog from Gaia and APOGEE (v_r , LSR; binned spatially according to the pixel sizes shown). The

Plot of spatially binned average radial velocities of the selected Gaia + APOGEE stars. The stars are distributed according to the regions of highest HI column density and display an east–west gradient in v_r with the same magnitude as seen in the T_b radial velocity map. The same East-West gradient appears



HI and stars velocity span the same range

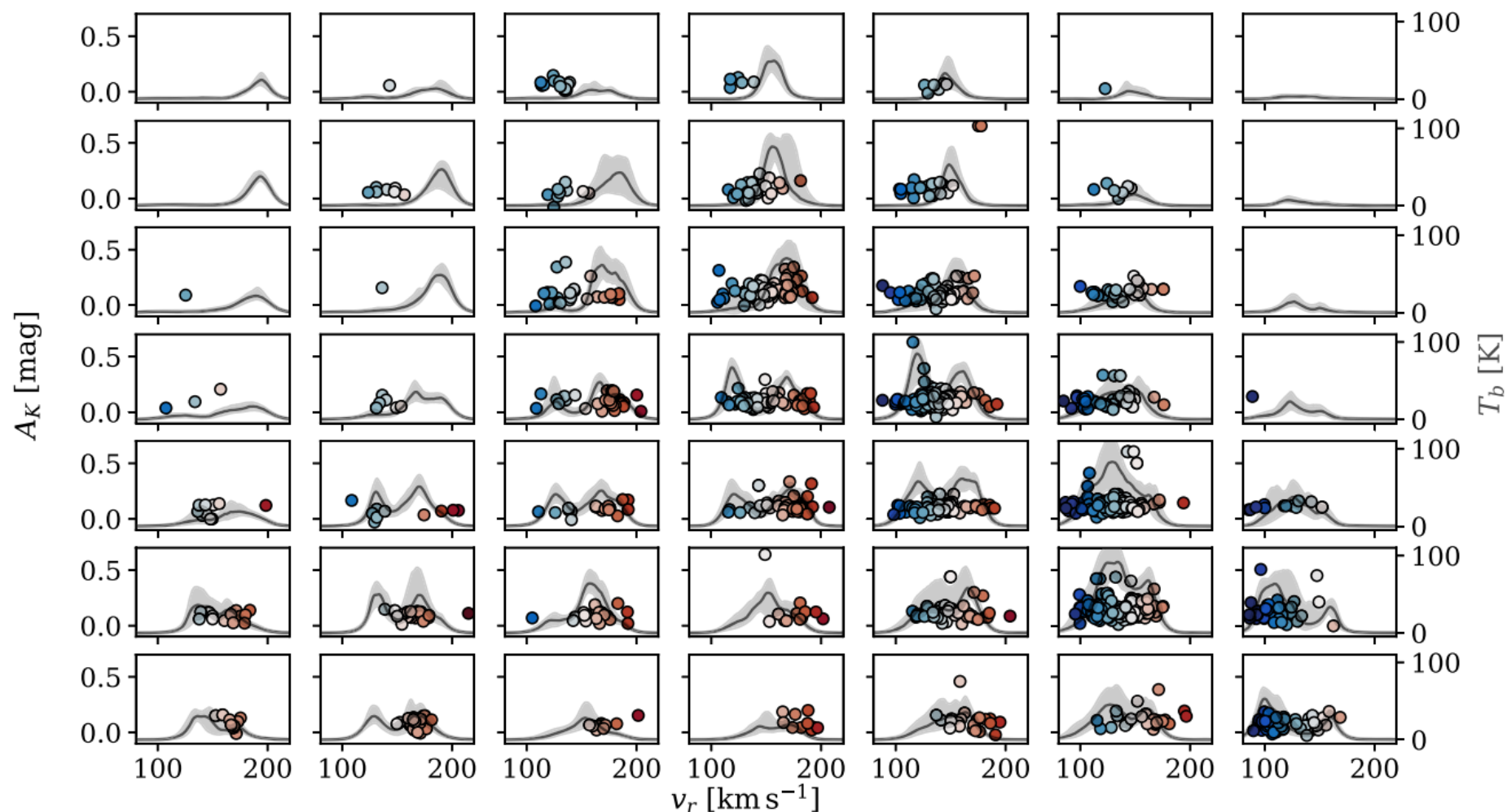


Figure 6. A_K vs. velocity for stars within the same regularly spaced spatial bins as in Figure 1. The stars are colored by the radial velocity according to the same color bar as in Figure 1. The average H I $T_b(v_r)$ profiles are overlaid in black and include shaded gray envelopes denoting the 16th–84th percentiles of the $T_b(v_r)$ within each spatial bin. In general, the stellar radial velocities span the same range as the H I velocities across the SMC.

Matching HI velocity structure and stars

- To match the stars with the HI peaks in the T_b distribution it is necessary to: 1) establish the number of HI components (two main components are found); 2) adopt a proper spatial binning of the stars (not homogeneously distributed across the field of view); 3) identify structures through differential extinction.
- About point 3): if in a given bin, there are at least two sources with low ($v_r < M_l$) and high velocity ($v_r > M_l$) -- M_l = intensity-weighted average radial velocity of the gas along the specific line of sight -- a differential extinction is computed and assigned to all the stars in that bin

$$\Delta A_K = \langle A_K \rangle_{\text{low}} - \langle A_K \rangle_{\text{high}}$$

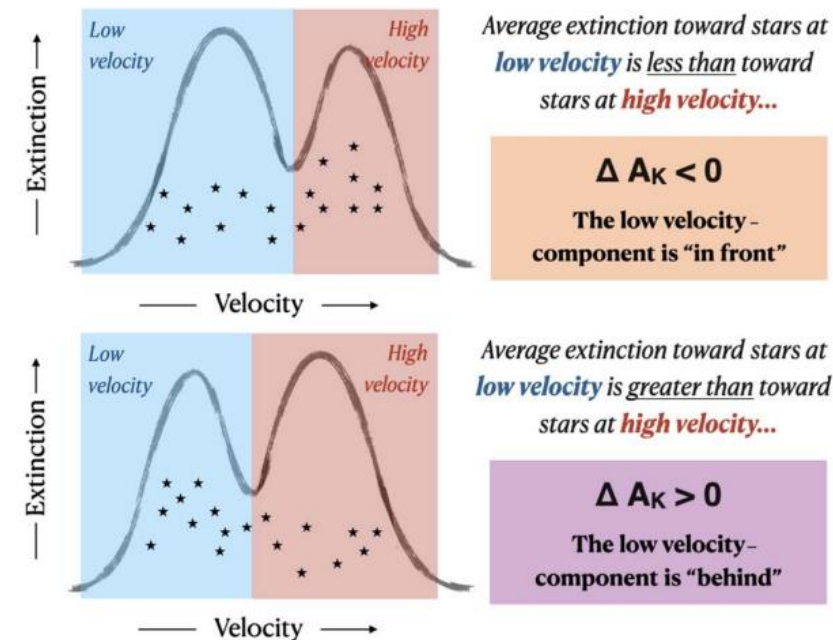


Figure 7. Cartoon schematic of the differential extinction estimation process. Top: the average extinction toward stars with low velocity ($v_r < M_l$) is less than the average extinction toward stars with high velocity ($v_r > M_l$); therefore, $\Delta A_K < 0$, and the low-velocity gas component is in front of the high-velocity component in this direction. Bottom: the average extinction toward stars with low velocity ($v_r < M_l$) is greater than the average extinction toward stars with high velocity ($v_r > M_l$); therefore, $\Delta A_K > 0$, and the low-velocity gas component is behind the high-velocity component in this direction.

Matching HI velocity structure and stars

- Clear trends are observed in the average differential extinction map: constant values across large areas of hundreds of parsecs indicates that the signal detected at each location is significant

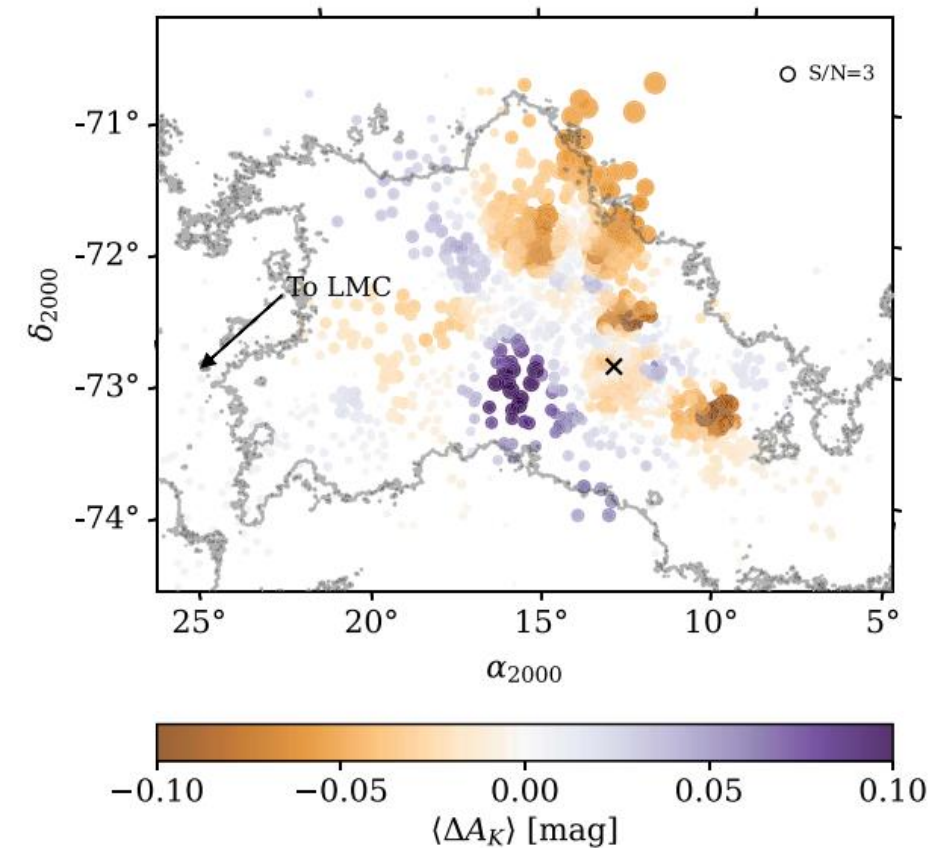


Figure 8. The difference in extinction toward low- and high-velocity gas ($\langle \Delta A_K \rangle$), averaged across binning parameters at the location of each source. The symbol sizes are scaled by the S/N in $\langle \Delta A_K \rangle$ (larger symbols = more confidence). The assumed center of the SMC is marked with a cross ($\alpha_0 = 13.15833$, $\delta_0 = -72.80028$; Zivick et al. 2021), and the direction toward the LMC is indicated with an arrow.

Matching HI velocity structure and stars

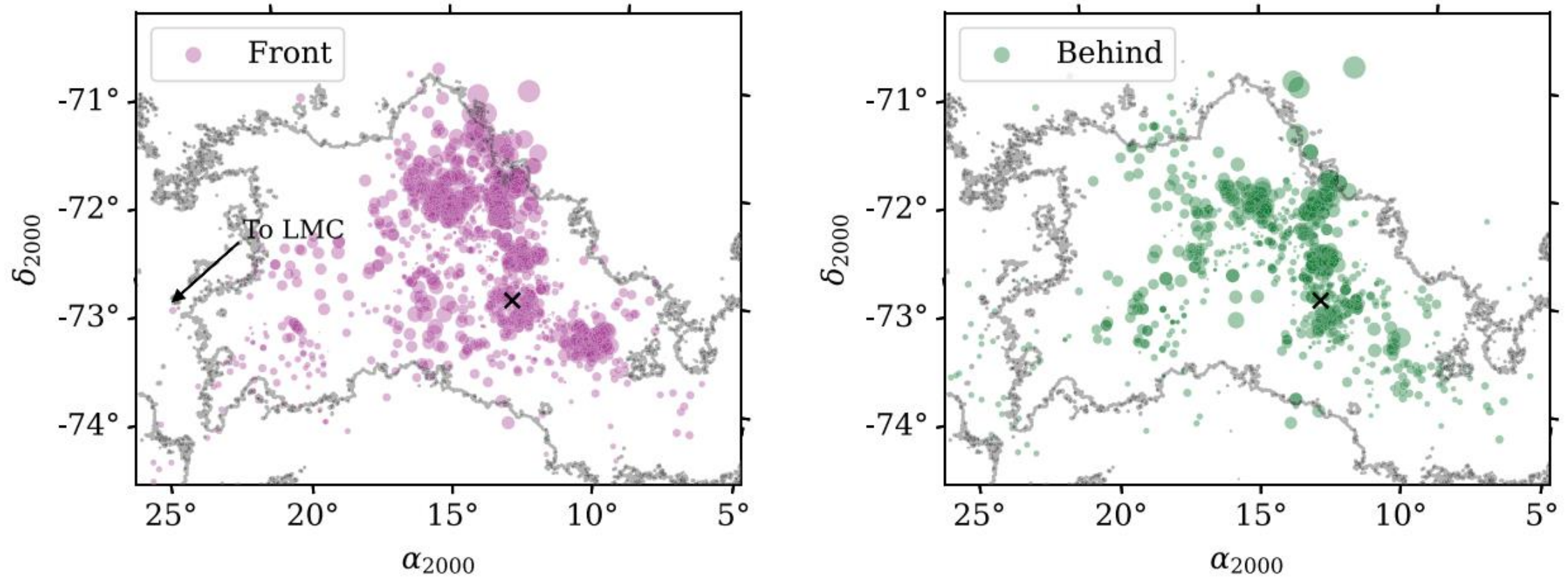


Figure 9. Spatial distribution of stars in the front structure ($\langle \Delta A_K \rangle < 0$ at low velocity and $\langle \Delta A_K \rangle > 0$ at high velocity) and the behind structure ($\langle \Delta A_K \rangle > 0$ at low velocity and $\langle \Delta A_K \rangle < 0$ at high velocity). As in Figure 8, the points are scaled by the significance in the $\langle \Delta A_K \rangle$ measurement.

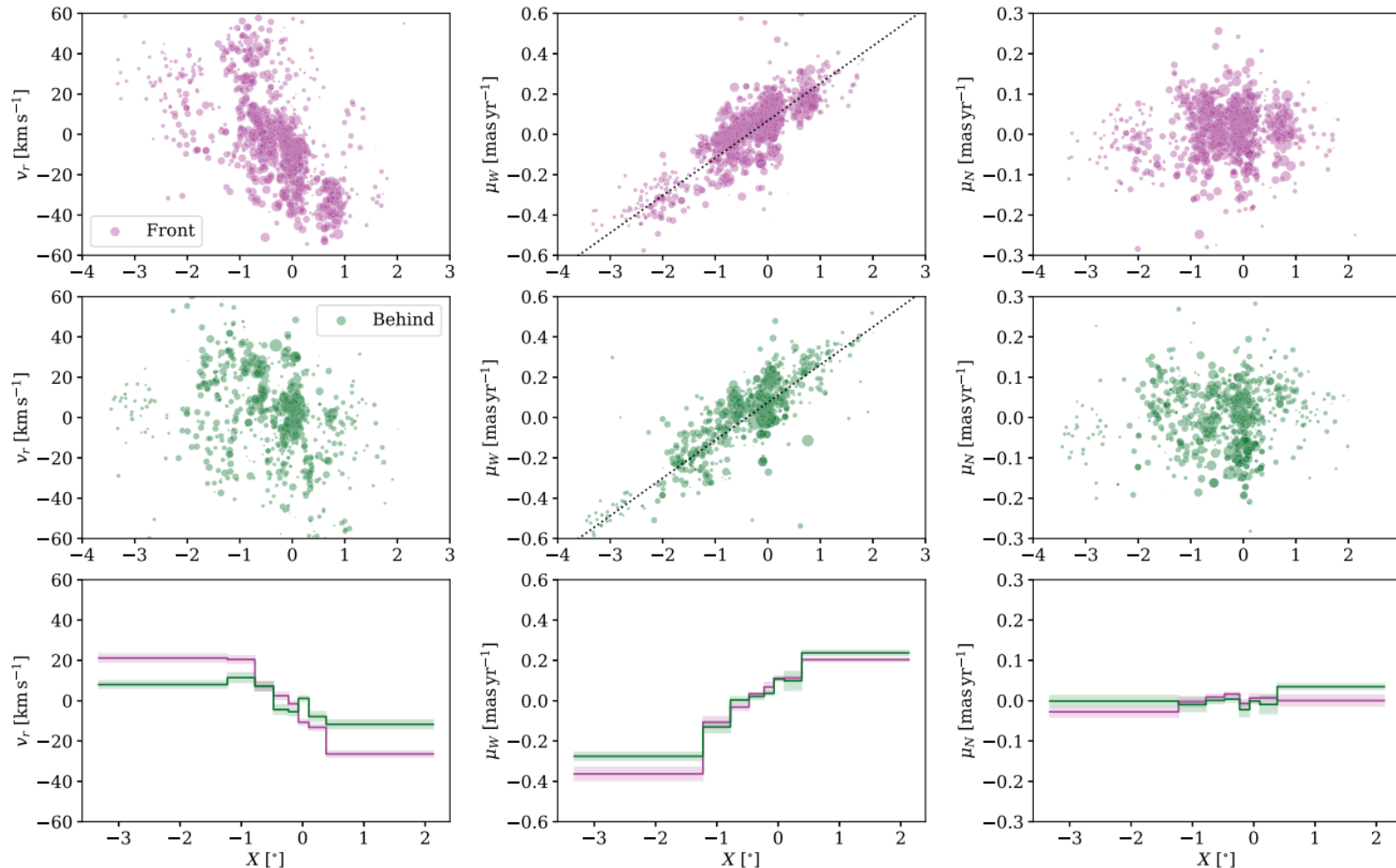


Figure 10. Comparing the 3D kinematics (v_r , μ_W , and μ_N ; left, middle, and right, respectively) as a function of the Cartesian east-west (X) position for stars in the front and behind structures after subtracting the systemic motions of the SMC. The bottom row of panels compares the binned average values for each velocity component in 10 bins of equal size for the front and behind structures, highlighting in particular the difference in v_r as a function of X .

- After a transformation of the reference system from Equatorial to Cartesian, and computing the residual wrt the systemic velocity trends are computed for the front and behind component in radial velocity East-West (μ_W) and North-South (μ_N) motion.

Kinematic features

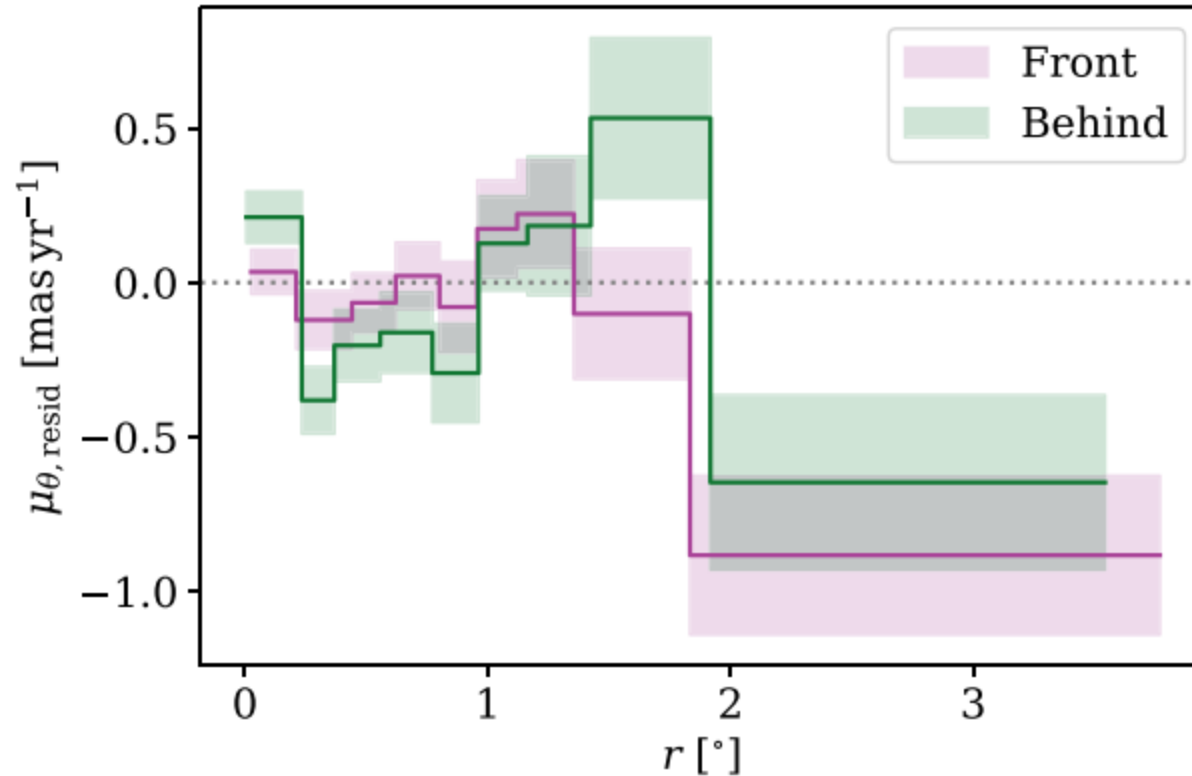


Figure 11. The residual tangential proper motion ($\mu_{\theta, \text{resid}}$) as a function of radius in the front and behind components after subtracting the gradient in μ_w (Figure 10). Here we plot the average (line) and standard error (shading) in bins of equal numbers of stars (six bins per sample).

- The residual tangential proper motion, obtained by subtracting the trends observed in the previous plots, indicate that the front and behind components are consistent with zero rotation in the innermost regions, while the front component has a consistently negative residual at larger radii, thus showing evidence of rotation. The behind component is distinct and shows a reverse trend.

Metallicity

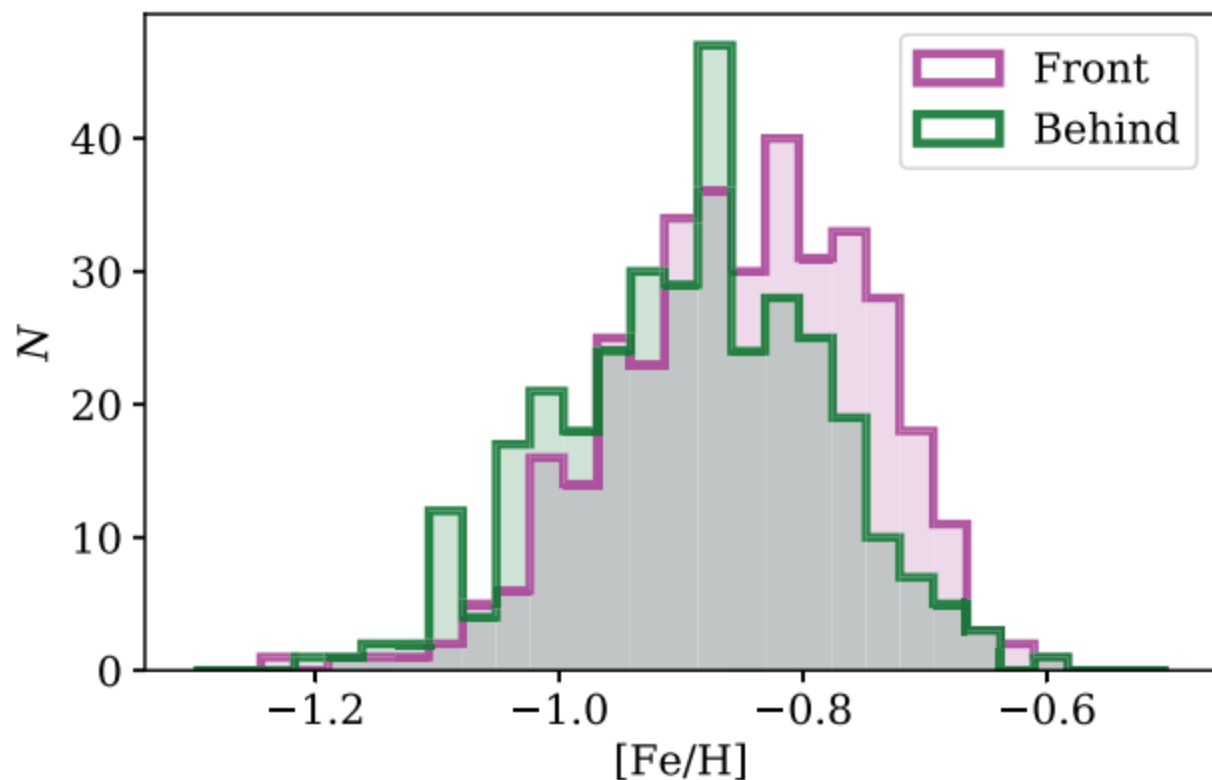


Figure 14. Histograms of $[Fe/H]$ for APOGEE stars in the front and behind components.

- APOGEE metallicity estimates allow to study the metallicity distribution in the front and behind samples. The two components span the same metallicity range but the the front component seems to have higher metallicity

Metallicity

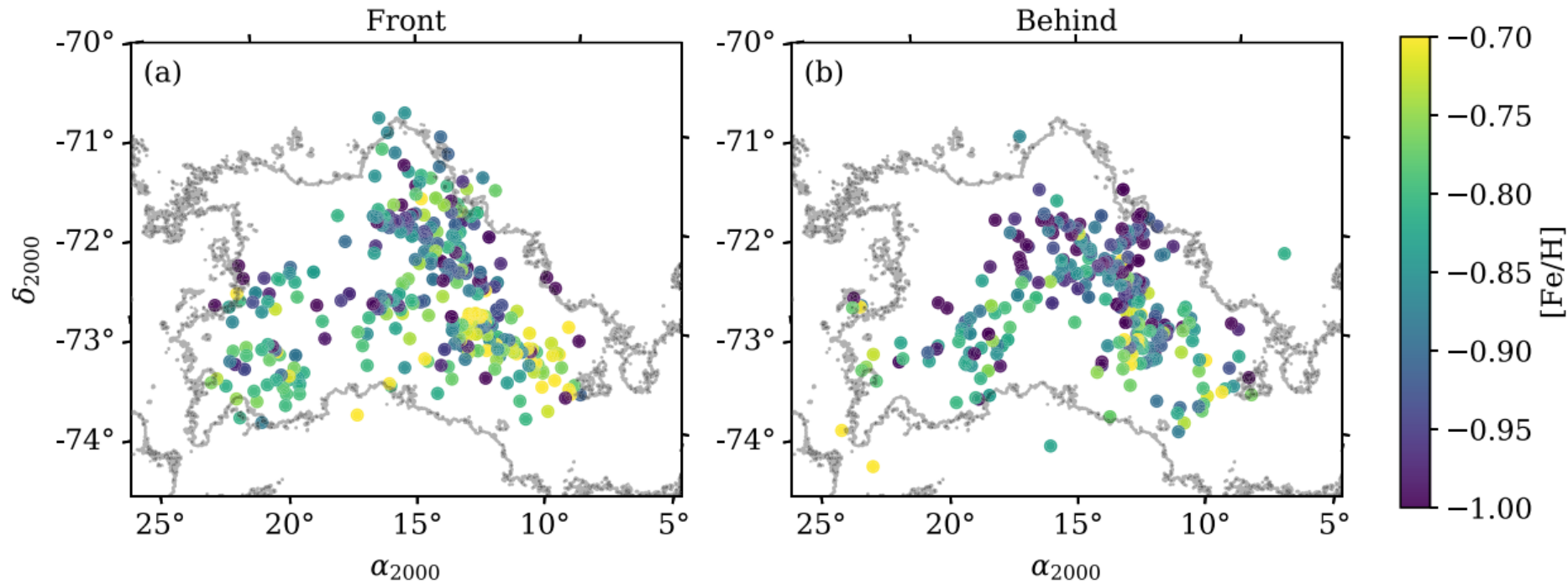


Figure 15. Spatial distribution of stars in the front (left) and behind (right) systems, colored by metallicity, $[Fe/H]$ (for those with estimates from APOGEE). The single contour denotes an HI column density of $15 \times 10^{20} \text{ cm}^{-2}$.

- The majority of high metallicity stars are located in the SW bar where most of the molecular gas and dust reside (Jameson+ 2016).
- The lowest metallicity stars are in the behind component in the Northern Bar: a possible explanation for this evidence is that (known) cold HI outflows from this region can form stars within, that will be more metal poor than those formed in the bar.

Conclusions



- a) The SMC young stellar population and ISM are not part of a simple rotating disk but are associated to distinct overlapping star forming systems (star lifetime 100 Myr). These systems cannot be simply classified as having low and high velocity due to the changes along the different lines of sight
- b) The SMC is likely consistent with two components separated by ~ 5 kpc, with the front component at ~ 61 kpc and the behind component at ~ 66 kpc
- c) Both the components are active star forming regions (traced by CO molecular gas) with stellar lifetimes of ~ 100 Myr, a time interval too short for young stars to be dynamically mixed – RSG are likely formed in the same systems where they are located today
- d) The dust geometry of the SMC follows the SW elongation of the bar, in agreement with previous studies
- e) Old stellar populations like Cepheids appear highly elongated and showing substructures that cannot be directly related with the ISM substructures observed in this work, although this fact highlights a possible connection with the existence of multiple components for the SMC

The results can be explained as:

- a) the components are the remnants of two different galaxies evolved in different ways (from differences in metallicities and molecular gas features, as well as non-uniform enrichment in the outskirts (Mucciarelli+ 2023))
- b) The front structure is the main galaxy and the behind structure is a debris resulting from the interaction with the LMC (bifurcated bridge and trailing Stream support this scenario, multiple HI (secondary) components)
- c) The behind component is a counter-bridge pulled from the interaction with the LMC (but the two components have similar HI mass, which is not expected in this scenario)